PAPER

Promising thermoelectric performance in n-type AgBiSe₂: effect of aliovalent anion doping†

Satya N. Guin,[a] Velaga Srihari[b] and Kanishka Biswas*[a]

Thermoelectric materials can convert untapped heat to electrical energy, and thus, it will have a significant role in future energy management. Recent industrial applications demand efficient thermoelectric materials which are made of non-toxic and inexpensive materials. Here, we report promising thermoelectric performance in halogen (Cl/Br/I) doped n-type bulk AgBiSe₂, which is a Pb-free material and consists of earth abundant elements. Aliovalent halide ion doping (2–4 mol%) in the Se²⁻ sublattice of AgBiSe₂ significantly increases the n-type carrier concentration in AgBiSe₂, thus improving the temperature dependent electronic transport properties. Temperature dependent cation order–disorder transition tailors the electronic transport properties in $AgBiSe_{1.98}X_{0.02}$ (X = Cl, Br and I) samples. Bond anharmonicity and disordered cation sublattice effectively scatter heat carrying phonon in the high temperature cubic phase of $AgBiSe_{1.98}X_{0.02}$ (X = Cl, Br and I), which limits the lattice thermal conductivity to a low value of ~0.27 W m⁻¹ K⁻¹ at 810 K. The highest thermoelectric figure of merit, *ZT*, value of ~0.9 at ~810 K has been achieved for the $AgBiSe_{1.98}Cl_{0.02}$ sample, which is promising among the n-type metal selenide based thermoelectric materials.

1. Introduction

Thermoelectric materials can directly and reversibly convert waste heat into electrical energy and are recognized as a renewable-energy source and a promising candidate to aid in the worldwide energy crisis.[1–9] The efficiency of thermoelectric materials is quantified by the dimensionless figure of merit (*ZT*), defined as $ZT = \sigma S^2 T/(\kappa_{el} + \kappa_{lat})$, where σ, S, T, κ_{el} and κ_{lat} are the electrical conductivity, Seebeck coefficient, temperature, electrical thermal conductivity, and lattice thermal conductivity, respectively.[1–9] Thermoelectric performance of an inorganic material could be improved either through enhancing the power factor ($S^2\sigma$) or through lowering the thermal conductivity or both at the same time.[1–9] Enhancement in the Seebeck coefficient can be achieved by electronic band structure engineering, such as introduction of resonance level in the electronic band,[10] band convergence,[11] quantum confinement effect,[12] and electron energy barrier filtering.[13] Significant

reduction of the thermal conductivity of bulk materials can be achieved by second phase nanostructuring[14] and all-length scale phonon scattering.[8] Alternatively, by utilizing critical phase transition behaviour[15] or intrinsically low thermal conductivity,[9] one can achieve high performance with single phase thermoelectric material.

Among the high performance power generation materials, lead chalcogenides are the best performers at mid/high temperatures, but environmental concern about Pb prevents its use in large-scale applications. Promising alternatives are a I–V–VI₂ (where I = Cu, Ag or alkali metal; V = Sb, Bi; and VI = S, Se, Te) class of semiconductor compounds.[16] These compounds exhibit intrinsically low κ_{lat} values due to strong anharmonicity in the bonding arrangements.[17] Recent theoretical and experimental studies on a series of bulk I–V–VI₂ compounds have shown that the lone pair on the group V element plays an important role in deforming the lattice vibration, results in strong anharmonicity, and thus gives rise to an ultralow thermal conductivity.[16] Ternary chalcogenide AgSbTe₂, which belong to the I–V–VI₂ family and its nanostructured alloys with GeTe (TAGS) and PbTe (LAST-m), are known for their remarkable *ZT* values.[14,18,19] Mention must be made that these high performance materials are generally based on tellurium which is extremely scarce in the Earth's crust.[20] Hence, the Te price is likely to rise sharply if Te-based thermoelectric materials reach mass markets. Attractive alternatives are Te-free AgSbSe₂ and AgBiSe₂. Recently, we have achieved *ZT* values more than unity in p-type 2 mol% Pb/Bi doped AgSbSe₂ and in p-type nanostructured AgSbSe₂–ZnSe samples.[21,22] Unexpectedly, most of the available high

[a]New Chemistry Unit, Jawaharlal Nehru Centre for Advanced Scientific Research (JNCASR), Jakkur P.O., Bangalore 560064, India. E-mail: kanishka@jncasr.ac.in

[b]Saha Institute of Nuclear Physics, 1/AF Bidhannagar, Kolkata 700064, India

† Electronic supplementary information (ESI) available: DSC data for AgBiSe₂ (Fig. S1), XPS spectra of $AgBiSe_{1.98}Cl_{0.02}$ (Fig. S2), EDAX elemental mapping of $AgBiSe_{1.98}Cl_{0.02}$ (Fig. S3), thermoelectric property data of 4 mol% halogen doped samples (Fig. S4), thermal diffusivity and heat capacity plot of 4 mol% halogen doped sample (Fig. S5), Lorentz numbers and electronic thermal conductivity (κ_{lat}) data (Fig. S6), total thermal conductivity estimated using measured and Dulong–Petit C_p (Fig. S7), room temperature κ_{total} and κ_{lat} value of present samples in comparison with the previously reported samples of AgBiSe₂ (Table S1).

performance materials are p-type; but both n-type and p-type materials are essential for constructing efficient thermoelectric module. To date, few compounds have evident n-type materials with ultra-low thermal conductivity.[23] $AgBiSe_2$ shows intrinsic n-type conduction in pristine bulk phase. Recently, a peak ZT value of ~1 at 773 K has been achieved in $AgBiSe_2$ by n-type Nb doping.[24] Surprisingly, solution grown $AgBiSe_2$ nanocrystals show p-type conduction with promising thermoelectric performance.[25] Although effect of the cation doping on the thermoelectric property of $AgBiSe_2$ have been investigated,[24] but the effect of anion substitution in this system is unexplored. Halide ion $(Cl^-/Br^-/I^-)$ can possibly aliovalently dope on the Se^{2-} sublattice and from simple valence counting, will contribute one n-type carrier in $AgBiSe_2$, which will improve the electronic transport property.

Here, we report the synthesis and promising thermoelectric properties of high quality bulk crystalline ingots of n-type $Cl^-/Br^-/I^-$ doped $AgBiSe_2$. We show that Cl^- acts as an effective n-type dopant and markedly increases the electrical conductivity up to ~340 S cm^{-1} at room temperature, which results in a large increase in the power factor $(S^2\sigma)$ of $AgBiSe_2$ over a wide temperature range. We could achieve a maximum ZT of ~0.9 at 805 K in the case of n-type $AgBiSe_{1.98}Cl_{0.2}$ crystalline ingot due to high power factor and intrinsically low thermal conductivity. In this article, we also report the comparison of the thermoelectric properties between Cl^-, Br^- and I^- doped $AgBiSe_2$ samples.

2. Experimental section

2.1 Materials

Elemental silver (Ag, 99.999%, metal basis), elemental bismuth (Bi, 99.9999%, metal basis), elemental selenium (Se, 99.999%, metal basis), bismuth chloride ($BiCl_3$, 99.999%, metal basis), bismuth bromide ($BiBr_3$, 99.999%, metal basis), bismuth iodide (BiI_3, 99.999%, metal basis) were purchased from Alfa Aesar and used for the synthesis without further purification.

2.2 Synthesis

Ingots (~9 g) of pristine $AgBiSe_2$ and $AgBiSe_{2-x}X_x$ (X = Cl/Br/I; x = 2–4 mol%) were synthesized by mixing appropriate ratios of high-purity starting materials of Ag, Bi, Se and BiX_3 (X = Cl/Br/I) in quartz tube. The tubes were sealed under high vacuum (~10^{-5} Torr) and slowly heated up to 673 K over 12 h, then heated up to 1123 K in 4 h, soaked for 10 h, and subsequently slow cooled to room temperature over a period of 12 h. For electrical and thermal transport measurements, the samples were cut and polished in bar and disk shape. Bar-shaped sample was used for simultaneous electrical conductivity and Seebeck coefficient measurement, whereas disk-shaped sample was used for thermal conductivity measurement.

2.3 Powder X-ray diffraction

Powder X-ray diffraction for all the samples were recorded using a laboratory Bruker D8 diffractometer with Cu K_α (λ = 1.5406 Å) radiation at room temperature. In order to get the information

about the structural phase transition, temperature dependent synchrotron X-ray diffraction measurements for pristine $AgBiSe_2$ has been carried out under N_2 flow with X-ray beam of E = 12.42 keV and λ = 0.998 Å, at BL-18B (Indian beam line), Photon Factory, KEK, Tsukuba, Japan. Energy of the beam was set by Si(111) double crystal monochromator, which was cross checked with Si (640b NIST) standard. All the measurements were carried out in Bragg–Brentano geometry with a divergence slit (300 μm), an anti-scattering slit (350 μm), and a receiving slit (300 μm). High temperature measurements were carried out with the Anton Paar DHS 1100 heat cell.

2.4 Band gap

To probe optical band gap, optical diffuse reflectance measurements have been performed on finely ground powders at room temperature. The spectra were recorded over the range of 200 nm to 3000 nm using a Perkin Elmer Lambda 900, UV/Vis/NIR spectrometer. Absorption (α/Λ) data were calculated from reflectance data using Kubelka–Munk equations: $\alpha/\Lambda = (1 - R)^2/(2R)$, where R is the reflectance, and α and Λ are the absorption and scattering coefficients, respectively.

2.5 Carrier concentrations

Room temperature carrier concentration of all the samples has been derived from Hall coefficient measurement by using PPMS (Physical Property Measurement System, Quantum Design, USA).

2.6 Electrical transport

Electrical conductivity and Seebeck coefficient were measured simultaneously under helium atmosphere from room temperature to ~823 K on a ULVAC RIKO ZEM-3 instrument system. The typical sample for measurement has a rectangular shape with the dimensions of ~2 mm × 2 mm × 8 mm. The longer direction coincides with the direction in which the thermal conductivity was measured. Heating and cooling cycles give repeatable electrical properties for a given sample.

2.7 Thermal transport

A Netzsch LFA-457 laser flash was used for thermal diffusivity, D, measurement in the range 300–823 K under N_2 atmosphere. Coins with ~8 mm diameter and ~2 mm thickness were used for all the measurements. Temperature dependent heat capacity, C_p, was derived using standard sample (pyroceram) in LFA457. The total thermal conductivity, κ_{total}, was calculated using the formula, $\kappa_{total} = DC_p\rho$, where ρ is the density of the sample, measured using sample dimension and mass. The density of the pellets obtained was in the range ~98% of the theoretical density. The error for the κ_{total} measurement is ~5%.

3. Results and discussion

Silver bismuth selenide, $AgBiSe_2$, is a polymorphous semiconductor known to show fascinating temperature dependent structural phase transition (Fig. 1(a)).[24,25] At room temperature,

$AgBiSe_2$ crystallizes in a cento-symmetric ordered hexagonal phase (space group $Pm\bar{3}1$; $a = 4.194$ Å, $c = 19.65$ Å). $AgBiSe_2$ undergoes two structural phase transitions at higher temperatures, ~460 K (hexagonal to rhombohedral) and ~580 K (rhombohedral to cubic), respectively.[24] The intermediate rhombohedral phase belongs to the $R\bar{3}m$ space group with the lattice constant of $a = 7.022$ Å, having ordered Ag and Bi atoms in the distinguishable positions, while in the high temperature cubic phase (space group $Fm\bar{3}m$, $a = 5.832$ Å), the Ag and Bi atoms are disordered.[26] In order to understand the structural phase transition in the present samples, we have performed temperature dependent (300–623 K) synchrotron powder X-ray diffraction (PXRD) of $AgBiSe_2$ (Fig. 1(b)). Temperature dependent PXRD data clearly indicates structural transition from rhombohedral to cubic phase above ~573 K, but the hexagonal to rhombohedral phase transition was not properly differentiated. Similar observation of structural phase transitions has been recorded in solution grown $AgBiSe_2$ nanocrystal and bulk $AgBiSe_2$ samples.[24,25] Differential scanning calorimetric (DSC) measurements (ESI, Fig. S1†) clearly shows a peak at ~585 K which is due to rhombohedral to cubic phase transition in $AgBiSe_2$. An onset ($T \sim 480$) of a low intensity peak has been

evidenced, which is near to the hexagonal to rhombohedral phase transition temperature.[24]

Room temperature powder XRD patterns of pristine $AgBiSe_2$ and $AgBiSe_{2-x}X_x$ (X = Cl, Br, I; $x = 2$–4 mol%) samples were measured in lab source (Cu K_α; $\lambda = 1.5406$ Å), which has been shown in Fig. 2. The XRD patterns of the all the halogen doped samples could be indexed based on room temperature hexagonal phase of $AgBiSe_2$ (space group $Pm\bar{3}1$), with no impurity phase being observed within the detection limits of powder XRD, which indicates successful substitution of halogen in the Se site of $AgBiSe_2$. Substitution of the halogen was further confirmed by X-ray photoelectron spectroscopy (ESI, Fig. S2†) and energy dispersive X-ray analysis (ESI, Fig. S3†) of the $AgBiSe_{1.98}Cl_{0.02}$ sample.

In Fig. 3, we have presented room temperature optical absorption spectra of pristine $AgBiSe_2$ and $AgBiSe_{1.98}X_{0.02}$ (X = Cl, Br and I) samples. The spectroscopically measured band gap of the pristine $AgBiSe_2$ is ~0.6 eV, which is typical of a narrow band gap semiconductor. Measured band gaps of $AgBiSe_{2-x}X_x$ (X = Cl, Br, I; $x = 2$ mol%) are slightly higher compared to that of pristine $AgBiSe_2$. The higher band gaps in halogen doped samples is due to higher electronegativity of the halogen
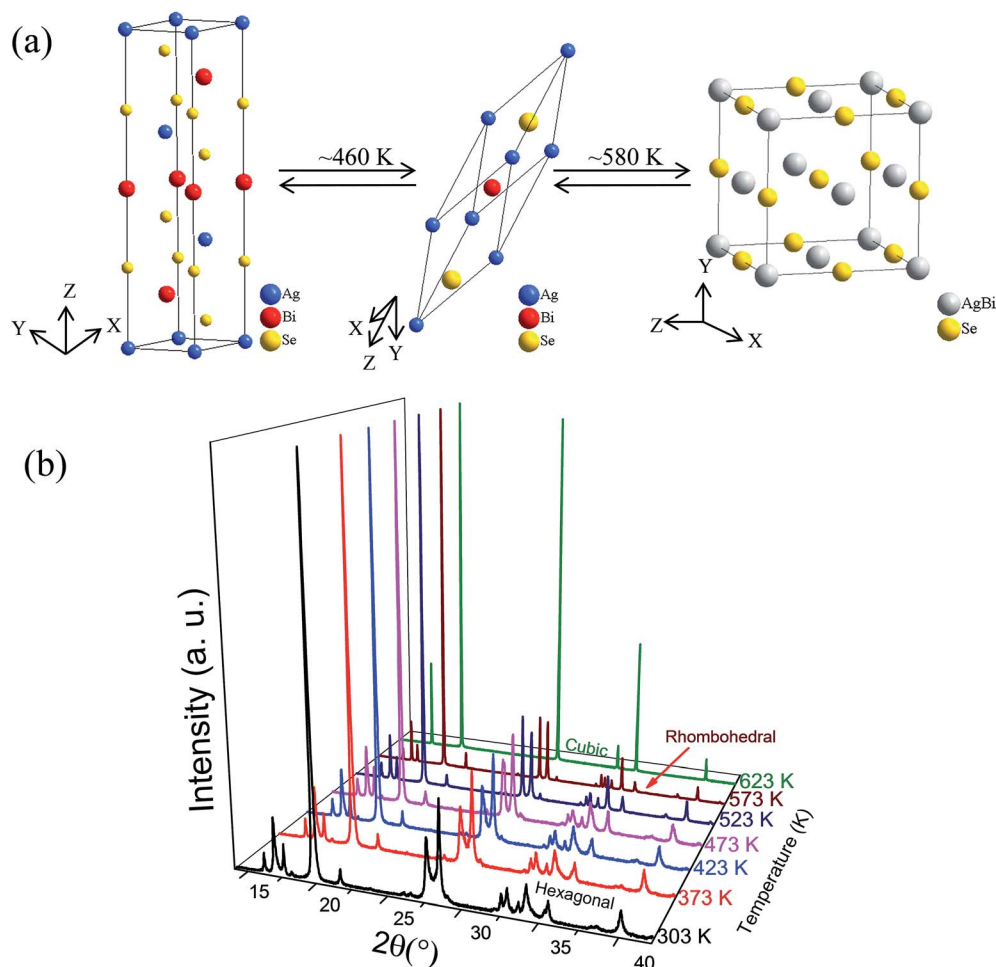

Fig. 1 (a) Temperature dependent crystal structure evaluation among hexagonal, rhombohedral and cubic phase of $AgBiSe_2$. (b) Temperature dependent synchrotron powder X-ray diffraction patterns ($E = 12.42$ KeV and $\lambda = 0.998$ Å) of $AgBiSe_2$.
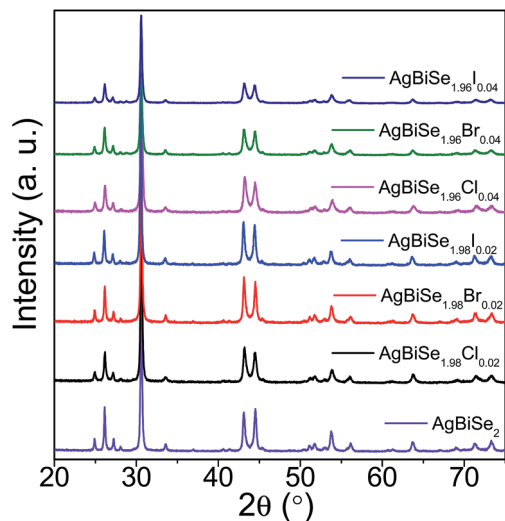
650 | J. Mater. Chem. A, 2015, 3, 648–655

This journal is © The Royal Society of Chemistry 2015

Fig. 2 Room temperature powder XRD pattern of pristine $AgBiSe_2$ and $AgBiSe_{2-x}X_x$ (X = Cl, Br, I; x = 2–4 mol%) recorded at lab source (Cu K_α; λ = 1.5406 Å).
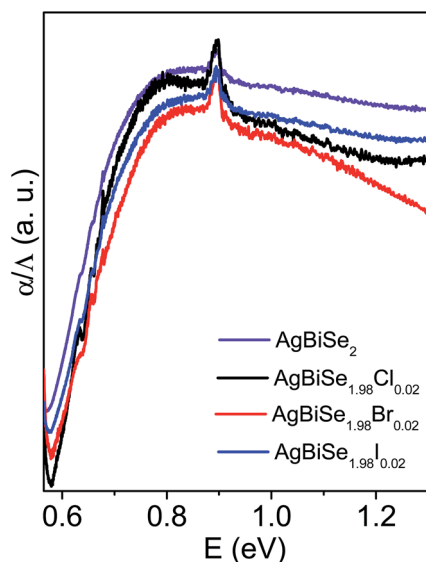
Fig. 3 Optical absorption spectra of pristine $AgBiSe_2$ and $AgBiSe_{1.98}$-$X_{0.02}$ (X = Cl, Br and I) samples.

Fig. 4 Temperature dependent (a) electrical conductivity (σ), (b) Seebeck coefficient (S), and (c) power factor (σS^2) of $AgBiSe_2$ and $AgBiSe_{1.98}X_{0.02}$ (X = Cl, Br and I) samples.

(Cl = 3.16, Br = 2.96, I = 2.66 in Pauling scale) compared to that of selenium (2.55). Thus, more ionic character of the metal–halogen bond than the metal–selenium bond results in widening the band gap of $AgBiSe_{1.98}X_{0.02}$ (X = Cl, Br, I). These results also support successful substitution of halogens in the Se site of $AgBiSe_2$.

Temperature dependent electronic transport properties of pristine $AgBiSe_2$ and $AgBiSe_{1.98}X_{0.02}$ (X = Cl, Br, I) samples have been presented in Fig. 4. In Fig. 4(a), we show temperature-dependent electrical conductivity (σ) of $AgBiSe_2$ and $AgBiSe_{1.98}X_{0.02}$ (X = Cl, Br, I) samples. A σ value of ~63 S cm^{-1} has been measured at room temperature in the case of pristine $AgBiSe_2$, which remains almost flat up to ~460 K (hexagonal to

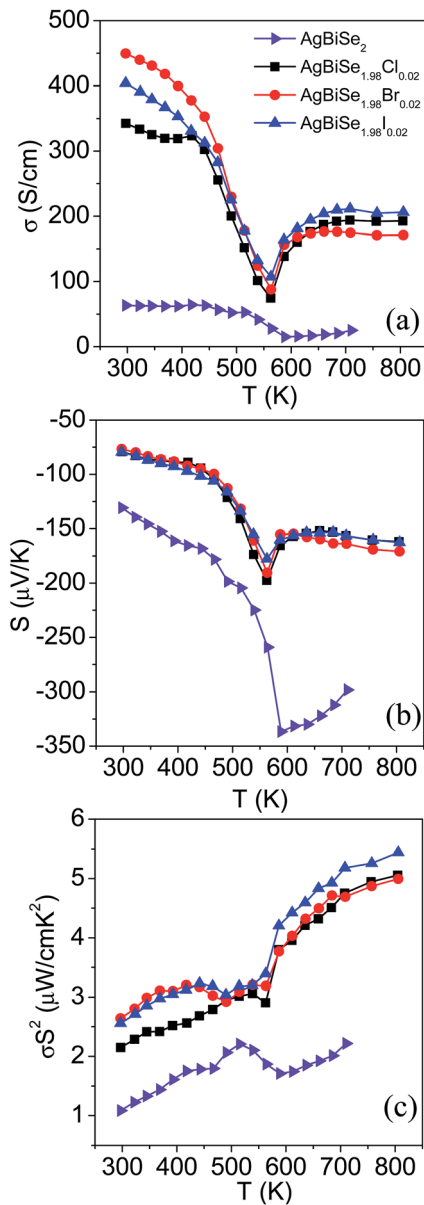rhombohedral phase transition temperature). In the rhombohedral phase (temperature range of 460–580 K), temperature dependent σ decreases continuously from ~52 S cm^{-1} to ~16 S cm^{-1} and behaves like metallic phase. $AgBiSe_2$ transforms to cubic phase around ~585 K, and then temperature dependent σ value increases to ~24 S cm^{-1} at 708 K. σ of 2 mol% halogen doped samples are significantly higher compared to that of pristine $AgBiSe_2$ sample. Typically, the $AgBiSe_{1.98}Cl_{0.02}$ sample shows a σ of ~343 S cm^{-1} at room temperature then decreases to ~300 S cm^{-1} at ~450 K (hexagonal to rhombohedral phase transition temperature). In the rhombohedral phase, temperature dependent σ decreases with increasing temperature and reaches a value of ~73 S cm^{-1} at ~562 K, indicating the metallic

behaviour. In the cubic phase of $AgBiSe_{1.98}Cl_{0.02}$, temperature dependent σ increases with increasing the temperature to reach a value of $\sim$193 S cm^{-1} at $\sim$810 K. Temperature dependent σ of $AgBiSe_{1.98}X_{0.02}$ (X = Cl, Br, I) samples shows typical metal to semiconductor transition during rhombohedral to cubic phase transformation. The room temperature σ of 2 mol% Br doped $AgBiSe_2$ sample is higher compared to that of 2 mol% Cl and I doped samples (see Table 1). The effective ionic radius of Cl$^-$, Br$^-$, I$^-$ and Se^{2-} are 1.81, 1.96, 2.20 and 1.98 Å respectively.[27] Thus, the higher value of σ measured for $AgBiSe_{1.98}Br_{0.02}$ sample is due to the perfect substitution of Br$^-$ ion in the Se^{2-} sublattice due to close matching of the ionic radius. Overall, the results indicate that halogen dopants can effectively enhance the electrical conductivity of $AgBiSe_2$ by doping electrons in the conduction band of $AgBiSe_2$. We have also investigated thermoelectric properties of $AgBiSe_{1.96}X_{0.04}$ (X = Cl, Br, I) samples (ESI, Fig. S4†). Room temperature σ for the 4 mol% Cl doped samples is higher than that of 2 mol% Cl doped $AgBiSe_2$ samples (Table 1), while the room temperature σ value of the 4 mol% Br/I doped samples is lower than that of 2 mol% Br/I doped $AgBiSe_2$ (Table 1).

The Hall coefficient, R_H, at room temperature is negative for pristine and halogen doped $AgBiSe_2$ samples, which indicates n-type conduction. Assuming parabolic bands and single band conduction process at 300 K, we have estimated the carrier concentration, n, from the formula: $n = 1/eR_H$, where e is the electronic charge. Measured carrier concentrations and carrier mobilities of pristine and halogen doped samples are presented in Table 1. Carrier concentration (n) increases from 5.85×10^{18} cm^{-3} for the pristine $AgBiSe_2$ to 3.72×10^{19} cm^{-3} for the $AgBiSe_{1.98}Cl_{0.02}$ sample. Carrier mobility (μ) decreases slightly for the 2 mol% halogen doped samples compared to that of pristine $AgBiSe_2$. Thus, the increase in the σ in 2 mol% halogen doped $AgBiSe_2$ is primarily due to an increase in the carrier concentration after halogen doping. Although 4 mol% halogen doped $AgBiSe_2$ samples show increased carrier concentration compared to 2 mol% halogen doped $AgBiSe_2$ samples, μ is lower in the case of 4 mol% halogen doped samples. The decrease of μ in 4 mol% halogen doped samples is due to excess charge carrier scattering from the point defects created by solid solution halogen doping.

In Fig. 4(b), we present temperature dependent Seebeck coefficient (S) of $AgBiSe_2$ and $AgBiSe_{1.98}X_{0.02}$ (X = Cl, Br, I)

samples. The negative sign of the S confirms the n-type conduction. The S value for pristine $AgBiSe_2$ is -131 μV K^{-1} at room temperature, which increases slowly with increasing temperature up to 460 K, and then within the rhombohedral phase, S increases quickly with increasing temperature to reach a value of -338 μV K^{-1} at $\sim$585 K. After the rhombohedral to cubic phase transition temperature, S reaches a value of -300 μV K^{-1} at $\sim$710 K. Halogen doping in $AgBiSe_2$ has a significant effect on the temperature dependent thermopower. All the halogen doped samples show lower S values compared to that of pristine $AgBiSe_2$ (Fig. 4(b)). The decrease in the Seebeck coefficient in halogen doped samples is due to increase in the carrier concentration in the system as, according to Mott–Jones formula, S is inversely proportional to the carrier concentration (n) and can be estimated as $S \sim n^{-2/3}$. Typically, $AgBiSe_{1.98}Cl_{0.02}$ samples show a S value of -81 μV K^{-1} at room temperature, which slowly increases with increasing the temperature up to hexagonal to rhombohedral phase transition temperature (460 K) then increases rapidly to reach a value of -198 μV K^{-1} at 562 K within the rhombohedral phase. In the cubic phase of $AgBiSe_{1.98}Cl_{0.02}$, temperature dependent S decreases initially after rhombohedral to cubic phase transition and then remains almost flat and shows a value of -163 μV K^{-1} at 810 K. Similar anomalies in the temperature dependent S have been observed in n-type Nb-doped $AgBiSe_2$ bulk ingot.[24] Mention must be made that solution grown p-type $AgBiSe_2$ nanocrystals show interesting reversible p–n–p type conduction (thermopower) switching,[25] which we have not observed in the present case.

Assuming single parabolic band model with acoustic phonon scattering ($r = -1/2$), we have estimated the carrier effective mass (m^*) values at room temperature according to the following eqn (1)–(3) using the measured S and Hall carrier concentration (n):

$$m^* = \frac{h^2}{2k_B T} \left[\frac{n}{4\pi F_{1/2}(\eta)} \right]^{2/3} \quad (1)$$

$$S = \pm \frac{k_B}{e} \left(\frac{(r+3/2)F_{r+3/2}(\eta)}{(r+3/2)F_{r+1/2}(\eta)} - \eta \right) \quad (2)$$

$$F_n(\eta) = \int_0^\infty \frac{x^n}{1 + e^{x-\eta}} \, dx \quad (3)$$

where η is the reduced Fermi energy, $F_n(\eta)$ is the nth order Fermi integral, k_B is the Boltzmann constant, e is the electron charge, h is the Planck constant, and r is the scattering factor. The reduced Fermi energy was extracted based on fitting the respective S vs. T data. The calculated m^* values for all the samples have been presented in Table 1. Calculated m^* values for the $AgBiSe_{2-x}X_x$ (X = Cl, Br, I; x = 2–4 mol%) samples are higher compared to that of bulk n-type BiAgSeS ($\sim$0.36 m_o) with rocksalt structure.[23]

Fig. 4(c) represents the temperature dependent power factors (σS^2) of the pristine and $AgBiSe_{1.98}X_{0.02}$ (X = Cl, Br, I) samples. A maximum σS^2 of $\sim$2.23 μW/cmK^2 at $\sim$708 K has been achieved for the pristine sample. σS^2 values for the halogen doped samples are significantly higher than that of the pristine sample. Typically, the $AgBiSe_{1.98}I_{0.02}$ sample shows a σS^2 value

Table 1 Room temperature carrier concentration (n), electrical conductivity (σ) carrier mobility (μ) and effective mass (m^*) of pristine $AgBiSe_2$ and $AgBiSe_{2-x}X_x$ (X = Cl, Br and x = 2–4 mol%) samples

Sample	n (cm^{-3})	σ (S cm^{-1})	μ (cm^2 V^{-1} S^{-1})	m^*/m_o
$AgBiSe_2$	5.85×10^{18}	63	67	0.25
$AgBiSe_{1.98}Cl_{0.02}$	3.72×10^{19}	343	57	0.46
$AgBiSe_{1.98}Br_{0.02}$	4.63×10^{19}	450	61	0.51
$AgBiSe_{1.98}I_{0.02}$	3.98×10^{19}	404	63	0.48
$AgBiSe_{1.96}Cl_{0.04}$	4.77×10^{19}	376	49	0.55
$AgBiSe_{1.96}Br_{0.04}$	4.60×10^{19}	337	46	0.54
$AgBiSe_{1.96}I_{0.04}$	4.65×10^{19}	196	26	0.59

of ~2.56 µW/cmK^2 at room temperature, which increases to a value of ~5.45 µW/cmK^2 at ~810 K. Superior electrical transport in the AgBiSe$_{1.98}$X$_{0.02}$ (X = Cl, Br, I) compared to the pristine AgBiSe$_2$ results in improved σS^2 in AgBiSe$_{1.98}$X$_{0.02}$ (X = Cl, Br, I) samples. The σS^2 values for the 4 mol% halogen doped samples are lower than that of 2 mol% halogen doped samples throughout the measured temperature range (ESI, Fig. S4†), which is primarily due to low σ values at low temperatures and low S values at high temperature.

The total thermal conductivity, κ_{total}, of pristine and AgBiSe$_{1.98}$X$_{0.02}$ (X = Cl, Br, I) samples was estimated over the 300–823 K temperature range using the formula, $\kappa_{total} = DC_p\rho$, where D is the thermal diffusivity, C_p is specific heat and ρ is density of the sample (Fig. 5). Temperature dependent D is measured by laser flash diffusivity technique over 300–823 K range (Fig. 5(a)). Temperature dependent C_p was derived during diffusivity measurement and plotted with Dulong–Petit C_p value (Fig. 5(b)). C_p values are consistent with the previously reported values of Nb-doped AgBiSe$_2$.[24] At room temperature, a κ_{total} value of ~0.77 W m^{-1} K^{-1} was measured for AgBiSe$_{1.98}$Cl$_{0.02}$, which remains almost same up to ~470 K (Fig. 5(c)). With further increase in temperature, within the rhombohedral phase, κ_{total} deceases with increasing temperature to reach a minimum value of ~0.52 W m^{-1} K^{-1} at ~570 K. Above the rhombohedral to cubic phase transition temperature (~575 K), κ_{total} of AgBiSe$_{1.98}$Cl$_{0.02}$ remains almost the same up to ~823 K. We have observed similar trend in the temperature dependent κ_{total} in Br/I doped AgBiSe$_2$ samples.

The lattice thermal conductivity, κ_{lat}, was obtained after subtracting the electronic thermal conductivity, κ_e, from the κ_{total} and plotted in Fig. 5(d). The electronic thermal conductivity (ESI, Fig. S6†) has been estimated using Wiedemann–Franz law: $\kappa_e = L\sigma T$, where Lorenz number, L, was extracted based on the fitting of the respective S values that estimate the reduced chemical potential, which was explained in detail elsewhere.[28] This assumes a parabolic band model and energy independent scattering time. Calculated Lorenz numbers for pristine and AgBiSe$_{2-x}$X$_x$ (X = Cl, Br, I; x = 2–4 mol%) samples are given in Fig. S6(a) in the ESI.† At room temperature, a typical κ_{lat} value of ~0.57 W m^{-1} K^{-1} was measured for AgBiSe$_{1.98}$Cl$_{0.02}$, which remains almost the same up to ~470 K (Fig. 5(d)). With further increase in the temperature to ~810 K, κ_{lat} deceases to reach a value of ~0.27 W m^{-1} K^{-1}. κ_{total} and κ_{lat} values of the present samples are comparable to the values reported in previous literature (ESI, Table S1†).[17,24] Measured low value of κ_{lat} above the order–disorder phase transition (rhombohedral-cubic) temperature (~570 K) is due to – (a) phonon softening owing to a high degree of anharmonicity of Bi–Se bonds caused by the stereochemically active lone pair ($6s^2$) on Bi and (b) effective phonon scattering by the disordered Ag/Bi lattice in the cubic phase of AgBiSe$_2$. 4 mol% halogen doped AgBiSe$_2$ samples also show reasonably low κ_{total} values throughout the measured temperature range (ESI, Fig. S4†).

Temperature dependent thermoelectric figure of merit, ZT, has been estimated from the measured electrical and thermal transport data in 300–810 K range for pristine and AgBiSe$_{1.98}$X$_{0.02}$ (X = Cl, Br, I) samples (Fig. 6). In Fig. 6(a), we show temperature dependent ZT values of pristine and AgBiSe$_{1.98}$X$_{0.02}$ (X = Cl, Br, I) samples, which were estimated using the C_p values measured during thermal diffusivity measurement. A peak ZT value of ~0.31 at 708 K has been achieved for pristine AgBiSe$_2$. Among the halogen doped samples, AgBiSe$_{1.98}$Cl$_{0.02}$ shows the highest ZT value with a peak ZT of ~0.75 at ~810 K. In the case of n-type bulk Nb-doped AgBiSe$_2$ samples, Dulong–Petit C_p was used for the calculation of temperature dependent ZT.[24] In order to compare the present ZT of halogen doped AgBiSe$_2$ with the ZT of previously reported Nb-doped AgBiSe$_2$ samples, we have also estimated the ZT of the AgBiSe$_{1.98}$Cl$_{0.02}$ sample using Dulong–Petit C_p, which has been presented in Fig. 6(b). A peak ZT value of ~0.9 at ~810 K has been achieved for the AgBiSe$_{1.98}$Cl$_{0.02}$ sample, which is comparable to the
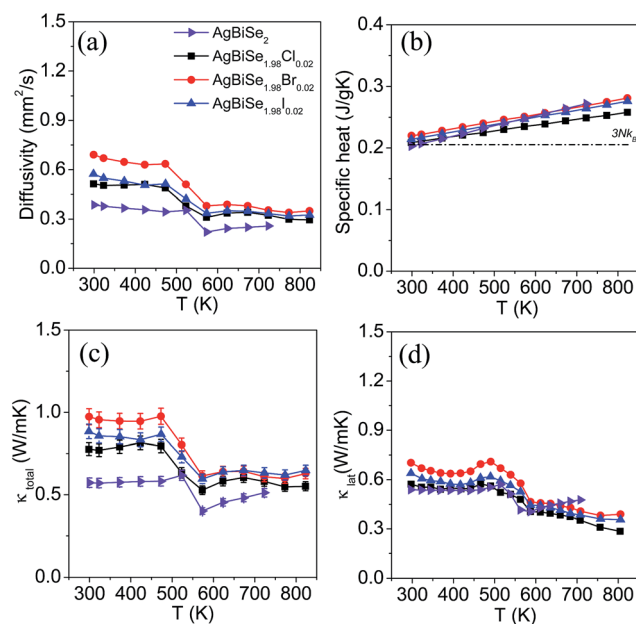

Fig. 5 Temperature dependent (a) thermal diffusivity (D), (b) specific heat (C_p), (c) total thermal conductivity (κ_{total}) with 5% error bar and (d) lattice thermal conductivity (κ_{lat}) of AgBiSe$_2$ and AgBiSe$_{1.98}$X$_{0.02}$ (X = Cl, Br and I) samples.
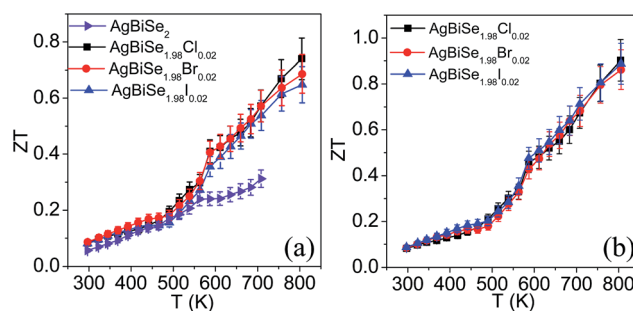
Fig. 6 (a) Temperature dependent thermoelectric figure merit (ZT) of AgBiSe$_2$ and AgBiSe$_{1.98}$X$_{0.02}$ (X = Cl, Br and I) samples estimated using measured C_p and (b) ZT of AgBiSe$_{1.98}$X$_{0.02}$ (X = Cl, Br and I) samples estimated using Dulong–Petit C_p. 10% error bar is shown for ZT estimation.

This journal is © The Royal Society of Chemistry 2015

J. Mater. Chem. A, 2015, **3**, 648–655 | 653

performance of previously reported Nb-doped $AgBiSe_2$ samples.[24] Thus, the present study indicates that high thermoelectric performance in n-type $AgBiSe_2$ can be achieved by aliovalent anion doping.

4. Conclusions

In conclusion, high quality crystalline ingots of n-type $AgBiSe_2$ and $AgBiSe_{2-x}X_x$ (X = Cl, Br, I; x = 2–4 mol%) were grown by simple melting of elemental metal and chalcogen followed by cooling to room temperature. Carrier concentrations in n-type $AgBiSe_2$ could be optimized by doping of a small amount of halogen in the Se sublattice of $AgBiSe_2$ to achieve superior electrical conductivity compared to the pristine sample. Halide ion ($Cl^-/Br^-/I^-$) aliovalently dopes on the Se^{2-} sublattice, and from simple valence counting, contributes one n-type carrier in $AgBiSe_2$, which gives rise to improved electronic transport property. Metal to semiconductor type transition is evidenced during rhombohedral to cubic phase transformation in halogen doped $AgBiSe_2$. The combination of enhanced electrical conductivity and a reasonably high Seebeck coefficient results in high power factor values peaking at high temperature of ~810 K. A high degree of anharmonicity in the Bi–Se bond, and effective phonon scattering by the disordered Ag/Bi lattice gives rise to ultra-low κ_{lat} in the cubic phase of $AgBiSe_2$. A peak ZT value of ~0.9 at ~810 K has been achieved for the $AgBiSe_{1.98}$-$Cl_{0.02}$ sample, which makes it a promising n-type thermoelectric material for mid-temperature applications. Further improvement of the performance of $AgBiSe_2$ could be achieved by either simultaneous improvement of the Seebeck coefficient and electrical conductivity or by introducing nanoscale precipitates and mesoscale grain boundaries.

Acknowledgements

Notes and references

1 L.-D. Zhao, V. P. Dravid and M. G. Kanatzidis, *Energy Environ. Sci.*, 2014, **7**, 251–268.

2 J. Sootsman, D. Y. Chung and M. G. Kanatzidis, *Angew. Chem., Int. Ed.*, 2009, **48**, 8616–8639.

3 G. J. Snyder and E. S. Toberer, *Nat. Mater.*, 2008, **7**, 105–114.

4 M. Zebarjadi, K. Esfarjani, M. S. Dresselhaus, Z. F. Ren and G. Chen, *Energy Environ. Sci.*, 2012, **5**, 5147–5162.

5 Y. Zhang and G. D. Stucky, *Chem. Mater.*, 2014, **26**, 837–848.

6 K. Nielsch, J. Bachmann, J. Kimling and H. Böttner, *Adv. Energy Mater.*, 2011, **1**, 713–731.

7 L. Hu, T. Zhu, X. Liu and X. Zhao, *Adv. Funct. Mater.*, 2014, **24**, 5211–5218.

8 K. Biswas, J. He, I. D. Blum, C. I. Wu, T. P. Hogan, D. N. Seidman, V. P. Dravid and M. G. Kanatzidis, *Nature*, 2012, **489**, 414–418.

9 L.-D. Zhao, S.-H. Lo, Y. Zhang, H. Sun, G. Tan, C. Uher, C. Wolverton, V. P. Dravid and M. G. Kanatzidis, *Nature*, 2014, **508**, 373–377.

10 (a) J. P. Heremans, V. Jovovic, E. S. Toberer, A. Saramat, K. Kurosaki, A. Charoenphakdee, S. Yamanaka and G. J. Snyder, *Science*, 2008, **321**, 554–557; (b) W. Liu, X. Tan, K. Yin, H. Liu, X. Tang, J. Shi, Q. Zhang and C. Uher, *Phys. Rev. Lett.*, 2012, **108**, 166601; (c) A. Banik and K. Biswas, *J. Mater. Chem. A*, 2014, **2**, 9620–9625.

11 Y. Pei, X. Shi, A. La Londe, H. Wang, L. Chen and G. J. Snyder, *Nature*, 2011, **473**, 66–69.

12 T. C. Harman, P. J. Taylor, M. P. Walsh and B. E. LaForge, *Science*, 2002, **297**, 2229–2232.

13 J. P. Heremans, C. M. Thrush and D. T. Morelli, *Phys. Rev. B: Condens. Matter Mater. Phys.*, 2004, **70**, 115334.

14 (a) K. Biswas, J. He, Q. Zhang, G. Wang, C. Uher, V. P. Dravid and M. G. Kanatzidis, *Nat. Chem.*, 2011, **3**, 160–166; (b) K. F. Hsu, S. Loo, F. Guo, W. Chen, J. S. Dyck, C. Uher, T. Hogan, E. K. Polychroniadis and M. G. Kanatzidis, *Science*, 2004, **303**, 818–821; (c) B. Poudel, Q. Hao, Y. Ma, Y. Lan, A. Minnich, B. Yu, X. Yan, D. Wang, A. Muto, D. Vashaee, X. Chen, J. Liu, M. S. Dresselhaus, G. Chen and Z. Ren, *Science*, 2008, **320**, 634–638; (d) H. J. Wu, L.-D. Zhao, F. S. Zheng, D. Wu, Y. L. Pei, X. Tong, M. G. Kanatzidis and J. Q. He, *Nat. Commun.*, 2014, **5**, 4515.

15 H. L. Liu, X. Yuan, P. Lu, X. Shi, F. F. Xu, Y. He, Y. S. Tang, S. Q. Bai, W. Q. Zhang, L. D. Chen, Y. Lin, L. Shi, H. Lin, X. Y. Gao, X. M. Zhang, H. Chi and C. Uher, *Adv. Mater.*, 2013, **25**, 6607–6612.

16 D. T. Morelli, V. Jovovic and J. P. Heremans, *Phys. Rev. Lett.*, 2008, **101**, 035901.

17 M. D. Nielsen, V. Ozolins and J. P. Heremans, *Energy Environ. Sci.*, 2013, **6**, 570–578.

18 F. D. Rosi, E. F. Hockings and N. E. Lindenblad, *RCA Rev.*, 1961, **22**, 82–121.

19 S. H. Yang, T. J. Zhu, T. Sun, J. He, S. N. Zhang and X. B. Zhao, *Nanotechnology*, 2008, **19**, 245707.

20 Z. C. Hu and S. Gao, *Chem. Geol.*, 2008, **253**, 205–221.

21 (a) S. N. Guin, A. Chatterjee, D. S. Negi, R. Datta and K. Biswas, *Energy Environ. Sci.*, 2013, **6**, 2603–2608; (b) S. N. Guin, A. Chatterjee and K. Biswas, *RSC Adv.*, 2014, **4**, 11811–11815.

22 S. N. Guin, D. S. Negi, R. Datta and K. Biswas, *J. Mater. Chem. A*, 2014, **2**, 4324–4331.

23 Y. L. Pei, H. Wu, J. Sui, J. Li, D. Berardan, C. Barreteau, L. Pan, N. Dragoe, W.-S. Liu, J. He and L. D. Zhao, *Energy Environ. Sci.*, 2013, **6**, 1750–1755.

24 L. Pan, D. Berardan and N. Dragoe, *J. Am. Chem. Soc.*, 2013, **135**, 4914–4917.

25 C. Xiao, X. Qin, J. Zhang, R. An, J. Xu, K. Li, B. Cao, J. Yang, B. Ye and Y. Xie, *J. Am. Chem. Soc.*, 2012, **134**, 18460–18466.

26 C. Manolikas and J. Spyridelis, *Mater. Res. Bull.*, 1977, **12**, 907–913.

27 R. D. Shannon, *Acta Crystallogr.*, 1976, **A32**, 751–767.

28 L. D. Zhao, H. J. Wu, S. Q. Hao, C. I. Wu, X. Y. Zhou, K. Biswas, J. Q. He, T. P. Hogan, C. Uher, C. Wolverton, V. P. Dravid and M. G. Kanatzidis, *Energy Environ. Sci.*, 2013, **6**, 3346–3355.